2017

Fabrication And Thermoelectric Characterization Of Stretchable Conductive Latex-Based Composites

Cory Michael Arcovitch
University of Vermont

FABRICATION AND THERMOELECTRIC CHARACTERIZATION OF STRETCHABLE CONDUCTIVE LATEX-BASED COMPOSITES

A Thesis Presented

by

Cory Arcovitch

to

The Faculty of the Graduate College

of

The University of Vermont

In Partial Fulfillment of the Requirements
for the Degree of Master of Science
Specializing in Mechanical Engineering

May, 2017

Defense Date: March 24th, 2017
Thesis Examination Committee:

Frederic Sansoz, Ph.D., Advisor
Matthew White, Ph.D., Chairperson
Patrick Lee, Ph.D.
Cynthia J. Forehand, Ph.D., Dean of the Graduate College

ABSTRACT

Miniaturized stretchable electronic devices that can be bent and strained elastically without breaking, have drawn considerable research interest in recent years for wearable computers and integrated bio-sensor applications. Portable electrical power harvesting remains a critical challenge in flexible electronics materials. One proposed solution has been to convert waste heat from the human body into electricity using thermoelectric materials. Traditionally, however, these materials are brittle ceramic semiconductors with limited fracture resistance under deformation. The primary objective of this thesis is to address this challenge by fabricating and studying the mechanical, thermal and electrical performance of stretchable composites combining natural latex polymer with either metallic (Ni) or thermoelectric (InSb) powders. Ni-based and InSb-based latex specimens were synthesized with different powder concentrations up to 36 vol.%. The effects of the powder concentration on tensile elongation, electrical conductivity, and thermal conductivity of the composites were measured at ambient temperature. Strong dependences of mechanical and electrical properties on powder concentration were found. By contrast, thermal conductivity was observed to remain low at all concentrations, suggesting that the predominant heat transport process is through the low-conductivity latex matrix rather than the conductive particles.

This thesis was conducted with the support of a Vermont Space Grant Consortium graduate research assistantship.

ACKNOWLEDGEMENTS

I would like to thank my advisor, Prof. Frederic Sansoz, for all the guidance and support he has given me throughout this journey. I don't think I could have chosen a better person to work with. He is kind, patient, and remarkably insightful. He has given me a deeper understanding of engineering and for that I have more gratitude and appreciation than I can express.

I would also like to thank my thesis committee, Prof. Patrick Lee and Prof. Matthew White, for their time, advice, and patience along the way. Their suggestions and attention to detail have made this work its best possible form. I cannot forget my Sansoz Research Group lab mates who were always there to help work through a problem or simply have a friendly conversation.

Finally, I would like to thank my vast support network including my girlfriend, Hayley, my best friend, Colby, my parents, my grandfather, and the rest of my family and friends who encouraged me, pushed me to do my best, and ultimately kept me sane throughout the process. This could not have been done without you.

This thesis was conducted with the support of a Vermont Space Grant Consortium graduate research assistantship.

TABLE OF CONTENTS

Page

LIST OF TABLES

Table Page

LIST OF FIGURES

Figure Page

CHAPTER 1: INTRODUCTION

Research in miniaturized stretchable electronic devices has become increasingly important for many applications including stretchable conductors [1, 2], wearable transistors [2], strain sensors [1, 3], and energy harvesters [4]. Fabricating smaller power systems for wearable electronics is of particular interest. A size-limiting factor for small electronic devices, however, is the trade-off between battery life and device size [5]. One proposed solution is to use thermoelectric (TE) materials to convert waste body heat into electrical power, but TE materials are typically stiff and brittle ceramic semiconductors that are impractical for wearable use. The primary objective of this thesis is to address this challenge by fabricating and studying the mechanical, thermal and electrical performance of stretchable composites combining natural latex polymer with either metallic (Ni) or thermoelectric (InSb) powders. Electrical, thermal and mechanical characterization at room temperature is performed to study the effects of powder concentration on electrical conductivity, thermal conductivity, and tensile elongation of the stretchable composites.

1.1. Stretchable Electronics

In recent years, considerable interest has been drawn into stretchable and flexible electronics for foldable computers and integrated bio-sensor applications [6, 7]. Silver nanowires (AgNWs) embedded into flexible polymer substrates, such as PDMS (Figure 1(a)), have shown promise as reliable stretchable conductors and capacitive strain sensors achieving a stable electrical conductivity at up to 50% tensile strain [1, 2, 3].

There are many ways researchers are achieving stable conductivity at high strains. Some include pre-straining the substrate before depositing NWs, nanoribbons, or thin films

[8, 9, 10, 11]. This buckles the surface at zero strain so when the substrate is strained, the NW network or film lays flat again instead of pulling apart and losing conductivity. Another method of creating stretchable electronics is strain-isolation and mesh configurations where small devices or circuits are interconnected with stretchable materials as a way to isolate the strain to only the interconnections [12, 13, 14]. This allows for otherwise brittle components to be arranged into a flexible and stretchable electronic device with only a slight loss in surface area.

Other methods include carbon nanotubes, graphene sheets, and small particles added to polymers, as well as more complex designs like serpentine configurations to allow for stretching, and woven fabric materials (Figure 1(b)) [4]. Furthermore, the above methods have been extended to stretchable energy harvesters by using piezoelectric, triboelectric, or thermoelectric materials [4, 15]. This thesis only focuses on thermoelectrics.

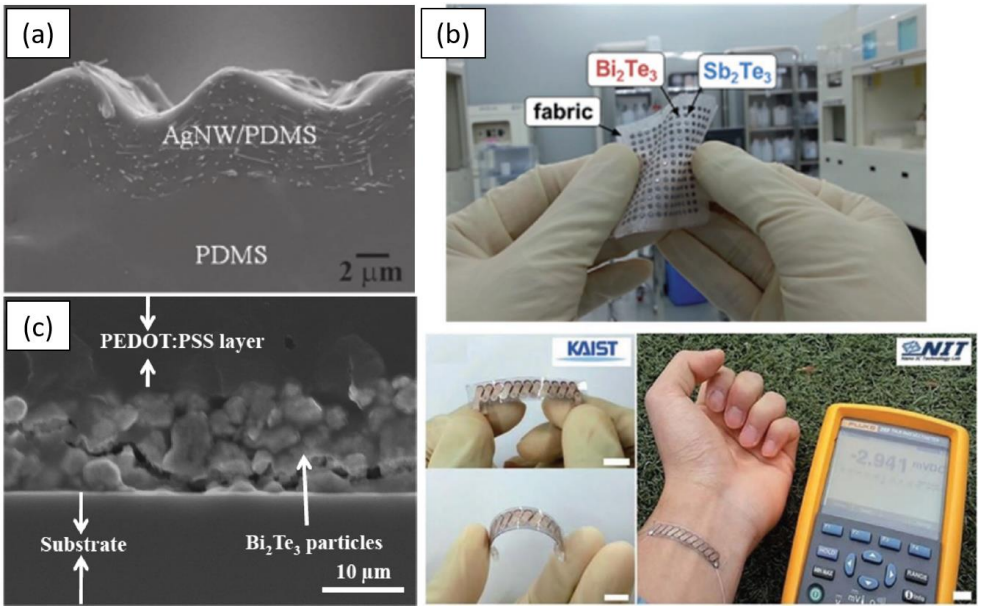

Figure 1: (a) A highly stretchable and flexible conductor made of AgNWs and PDMS [1]. (b) A flexible TE generator on a woven glass fabric [16]. (c) A TE composite made of Bi_2Te_3 particles and PEDOT:PSS conductive polymer [17].

1.2. Thermoelectric Materials

Thermoelectric materials are capable of direct energy conversion between heat and electricity and vice versa. Thermoelectric conversion relates to the dimensionless figure of merit $ZT=\sigma S^2 T/\lambda$ as a function of electrical conductivity (σ), Seebeck coefficient (S), thermal conductivity (λ), and temperature (T). To maximize ZT, one must increase σ and S or decrease k. However, trying to optimize one property may negatively affect a different property, i.e. insulating the material to reduce thermal conductivity may also result in decreasing the electrical conductivity [18]. Therefore, to effectively increase ZT, the overall ratio of electrical conductivity to thermal conductivity must increase.

Bi_2Te_3 material exhibits one of the highest ZT at room temperature, and consequently has been highly characterized in the literature [19, 20, 21]. This thesis will investigate a less common but still promising TE material, Indium Antimonide (InSb), because it has the highest carrier mobility of all III-V semiconductors. The maximum ZT value for bulk InSb was found to be 0.6 at 673K [22]. For practical TE devices, a material with $ZT > 1$ is desirable [22, 23]. Therefore, InSb is a strong candidate, as it does not need to be greatly improved to reach that goal.

1.3. Stretchable Thermoelectric Devices

Current applications for TE devices include power systems (radioisotope TE generator) for satellites too far out into space for solar cells to be effective [24] (Figure 2) and solid-state cooling devices such as wine coolers. However, common TE materials are heavy, stiff, and brittle ceramics with limited fracture resistance under deformation. It has been shown that TE generators can outperform solar cells on a typical person with

obtainable power ~ 30-37 μW/cm^2 of a person's skin at room temperature while indoors [25]. Another study found that a small TE device on a person's neck could harvest 0.20-0.32 W [5]. If TE materials could have the stretchability and flexibility of polymers while maintaining good TE properties, they could become more relevant for applications with complex geometry, or requiring large strains and bending deformation, including flexible waste-heat energy harvesters [15]. One possible way to give TE materials stretchability is to make a composite of a polymer and TE powder. Zhang et al. showed that a TE powder, Bi_2Te_3, mixed with a conductive polymer, PEDOT:PSS (Figure 1(c)), had promising TE properties and maintained flexibility [17].

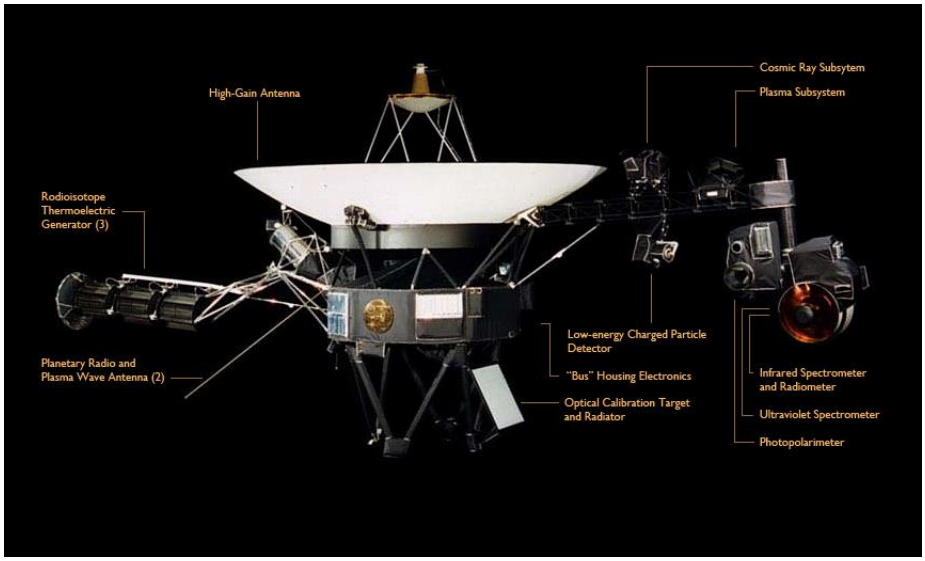

Figure 2: Voyager satellite components showing radioisotope TE generator as power source [24].

1.4. Objective of the Thesis

The objective of this thesis is to investigate the effects of conductive powder concentrations on mechanical, thermal and electrical properties at room temperature in stretchable composites combining natural latex polymer with either metallic (Ni) or thermoelectric (InSb) powders.

CHAPTER 2: EXPERIMENTAL METHODS

2.1. Fabrication

TAP Premium Liquid Latex Rubber was mixed with Buehler Conductive Ni Filler for the Ni-Latex composites and American Elements -325 Mesh, high purity InSb powder for the InSb-Latex composites. For both types of composites, the latex and powder were weighed out and mixed together in a 100-mL beaker with a metal scoopula until the mixture appeared homogeneous. DI water was added in intervals of 1mL until thin enough to be poured into a mold. InSb fabrication was conducted in a fume hood.

Three different molds were made as shown in Figure 3. For electrical testing, the bottom of a Gel-Pak Gel-Box with PDMS removed was used. This mold led to thin and flat specimens (~1.5 mm) good for cutting and measuring resistance. A deeper square mold was created out of PET film and electrical tape to make a thicker sample for thermal testing that required a larger probing depth (~5 mm). A third mold was in the shape of a dog bone specimen for tensile testing. A 3D CAD model was made in SolidWorks and then printed with a MakerBot Replicator in the UVM Fab Lab. The 3D printed part was then cast in PDMS to create the mold.

First, Ni-latex samples were prepared using different weights of powder (wt.%) based on the weight of Ni and liquid latex mixed together, ranging from 40 wt.% Ni to 70 wt.% Ni, in increments of 10 wt.%. When the InSb samples were made, however, comparison in wt.% was no longer justified because of the difference in density between Ni and InSb, 8,880 kg/m^3 and 5,775 kg/m^3 [26, 27], respectively. Therefore, the ratio of those two densities (~0.65) was used to determine the weight of InSb to be mixed with the same weight of latex to create samples that matched approximately with the volume

fraction (vol.%) of Ni powder. The theoretical vol.% for these samples was calculated using the material densities along with the density of latex, 930 kg/m^3 [28], accounting for the fact that the liquid latex used is only 74 wt.% latex solids and assuming all water evaporates during drying. Volumes of the two components were determined by dividing weight by the density. The error associated with this method was estimated to be < 5 vol.%, including scale accuracy (0.1g) and residual water concentration if not all water evaporates.

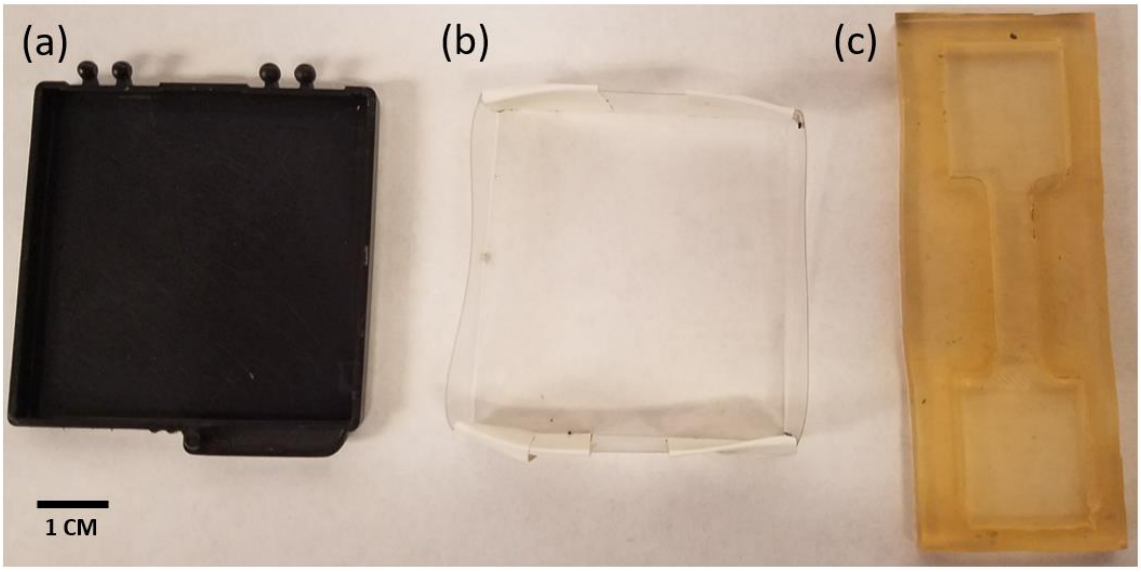

Figure 3: Three types of molds used for (a) electrical, (b) thermal, and (c) mechanical characterization.

Table 1 shows a breakdown of samples prepared for this thesis. Different vol.% were investigated for each type of powder. Due to our interest for investigating thermal-electrical properties at same vol.%, samples that exhibited no electrical conductivity at all were not investigated further and are listed as "N/A" in Table 1. We note that the 25 vol.% Ni tensile specimen is shown in Table 1 as "Failed" because all attempts resulted in the sample forming too many cracks and falling apart while drying.

Table 1: Breakdown of fabricated specimens by powder, wt.%, vol.%, and specimen type.

Material	Powder (wt.%)	Liquid Latex (wt.%)	Added Water (wt.%)	Powder Vol% (dry)	Electrical	Thermal	Mechanical
Ni	33	50	17	9	X	N/A	X
	43	43	14	12	X	X	X
	53	35	12	17	X	X	X
	58	25	17	25	X	N/A	Failed
InSb	42	43	15	17	X	X	N/A
	48	31	21	25	X	X	X
	61	23	16	36	X	X	X

2.2 Characterization

2.2.1. Microstructure

Microstructure imaging was performed on a JEOL JSM 6060 Scanning Electron Microscope (SEM). Small pieces were cut from the electrical specimens with scissors and imaged. Initially the voltage was set to 15 kV, but due to charging in the latex, it was dropped to 5 kV. A cross-sectional image was also taken of the 25 vol.% InSb specimen to determine if the powder had settled during drying.

Image analysis was performed with Gwyddion software [29] to attempt to verify the theoretical vol.% of powder. A threshold can be set on an image to highlight areas above or below a set spot on the greyscale. We created a mask that highlighted all the particles on or above the surface but not below it. For many images, the mask had to be manually modified due to the software applying the mask on charging areas of latex or on particles below the surface. Once the mask was considered satisfactory, the software provided the percent area covered by the mask as well as a distribution of particle size. This was done for five images, averaged, and compared to the theoretical vol.% at 17 vol.%.

2.2.2. Electrical Testing

Electrical testing was performed at ambient temperature using a Keithley 2400 SourceMeter source measure unit. This unit has an overflow limit of measurable resistance of 20MΩ. Specimens beyond that threshold were measured with a Novocontrol Alpha-AT impedance analyzer with a much higher limit to see if they were conductive at all. The square electrical specimens were cut with scissors into three randomly sized rectangles and their resistances were measured. Various ways of connecting the specimens to the machine were attempted starting with using copper tape attached to the specimen. The alligator clips from the source meter were then clamped on the copper tape. However, the adhesive on the tape reacted with the latex creating a black residue and unstable results. Silver paint adhesive was then applied to both sides of the specimen and attached to the copper tape while still wet to adhere to the copper. This improved the contact and the results, but the silver was very brittle and would break off while trying to attach the clamps. So instead, 12mm Al SEM specimen mounts were used as plate electrodes as shown in Figure 4.

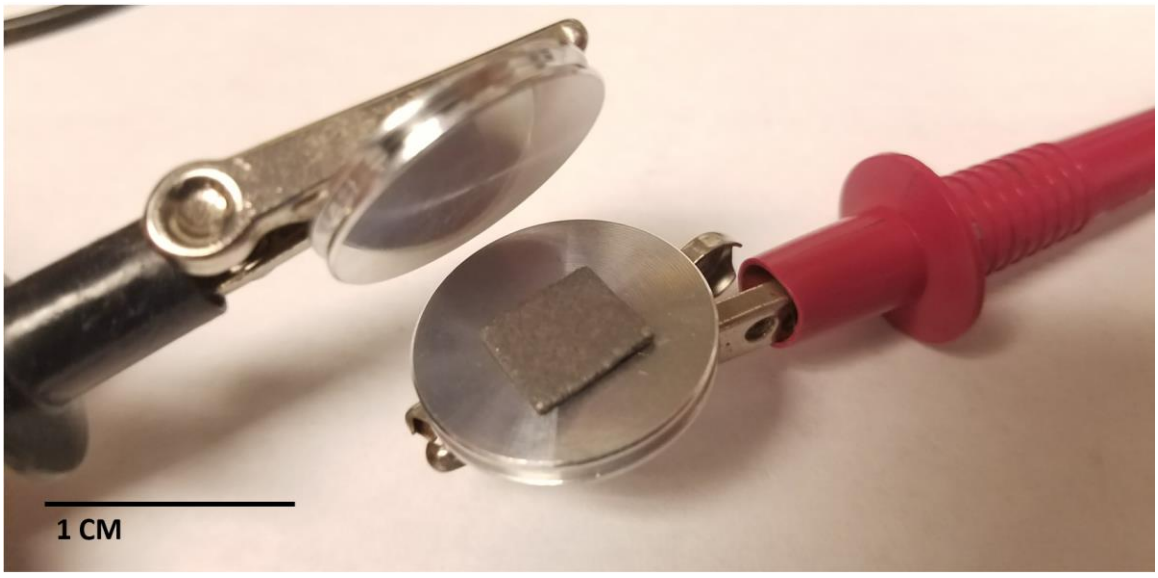

Figure 4: Image of electrical measurement setup showing specimen on Aluminum SEM specimen mounts acting as plate electrodes. These clamps are connected to the Keithley SourceMeter to measure resistance.

The contact resistance for this setup was measured to be ~0.15 Ω by touching the two plates together with no specimen in between and recording the resistance. This value is less than 1% of the most electrically conductive specimens and therefore treated as negligible. The dimensions of the specimens were measured using a Johnson Level 1889-0600 6" digital calipers with an accuracy of 10 microns. The electrical conductivity was calculated with the following equation:

$$\sigma = t/RA \qquad (1)$$

where t is the specimen thickness, R is the measured resistance, and A is the cross-sectional area. Any error in measurement of the specimen is assumed to be encapsulated by the error in averaging measurements on three samples.

2.2.3. Thermal Testing

Thermal testing was performed using a Thermtest transient Hot-Disk TPS 2200 Thermal Constants Analyzer (Figure 5). Bulk thermal conductivity was measured for each concentration. For InSb at the two highest concentrations, axial and radial measurements were also performed to study any anisotropy. This involved first measuring the volumetric heat capacity using a specific heat module and gold cell sensor. Once the setup was completed and the correct parameters were chosen [30], five measurements were taken automatically.

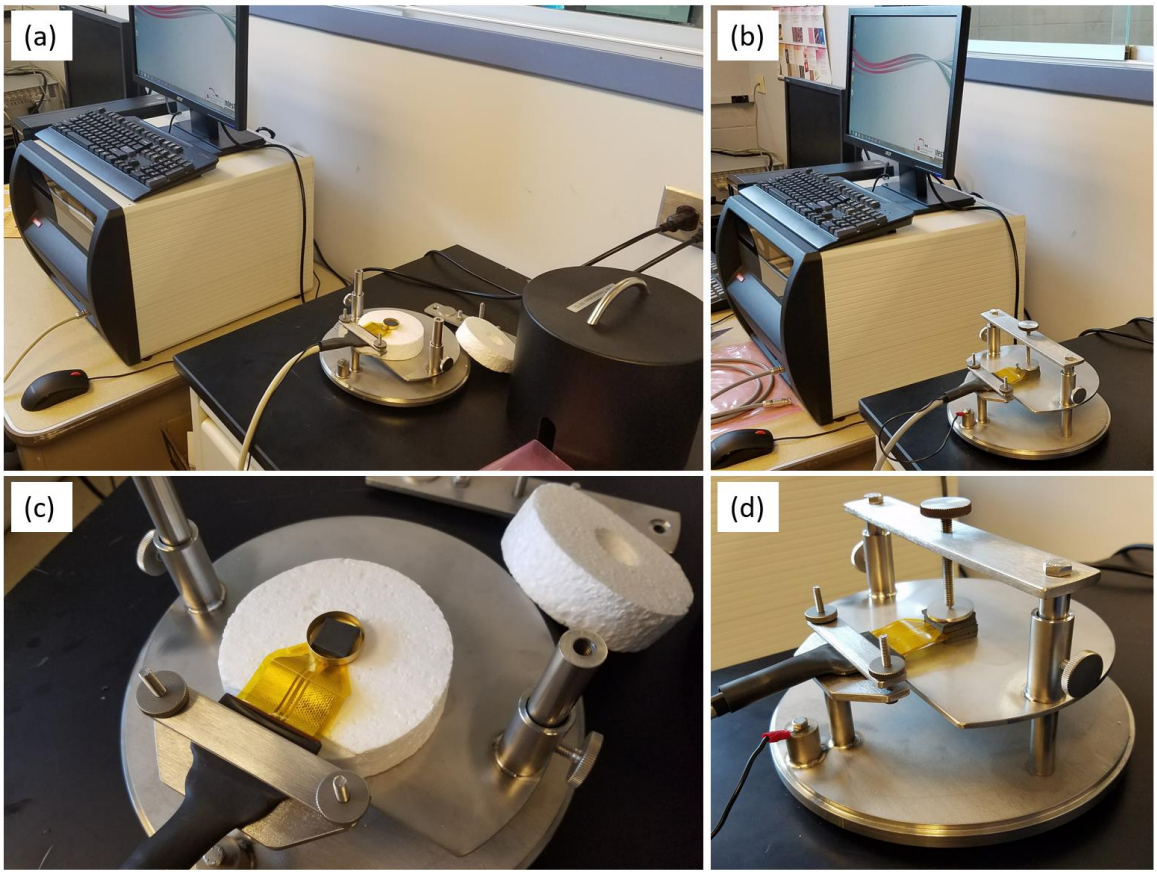

Figure 5: (a) and (b) show the TPS 2200 Thermal Constants Analyzer setup for the specific heat and thermal conductivity measurements, respectively. (c) and (d) are close ups of those setups with InSb-latex.

2.2.4. Mechanical Testing

Tensile testing was performed on a Test Resources 1000M single column testing machine to study how powder additions affected the elasticity of the latex matrix. The tests were performed on the dog bone specimens with a strain rate of 1in/min. Copper tape was wrapped around the ends of the specimen to prevent slipping in the vice during testing. The specimen shape and setup can be seen in Figure 6.

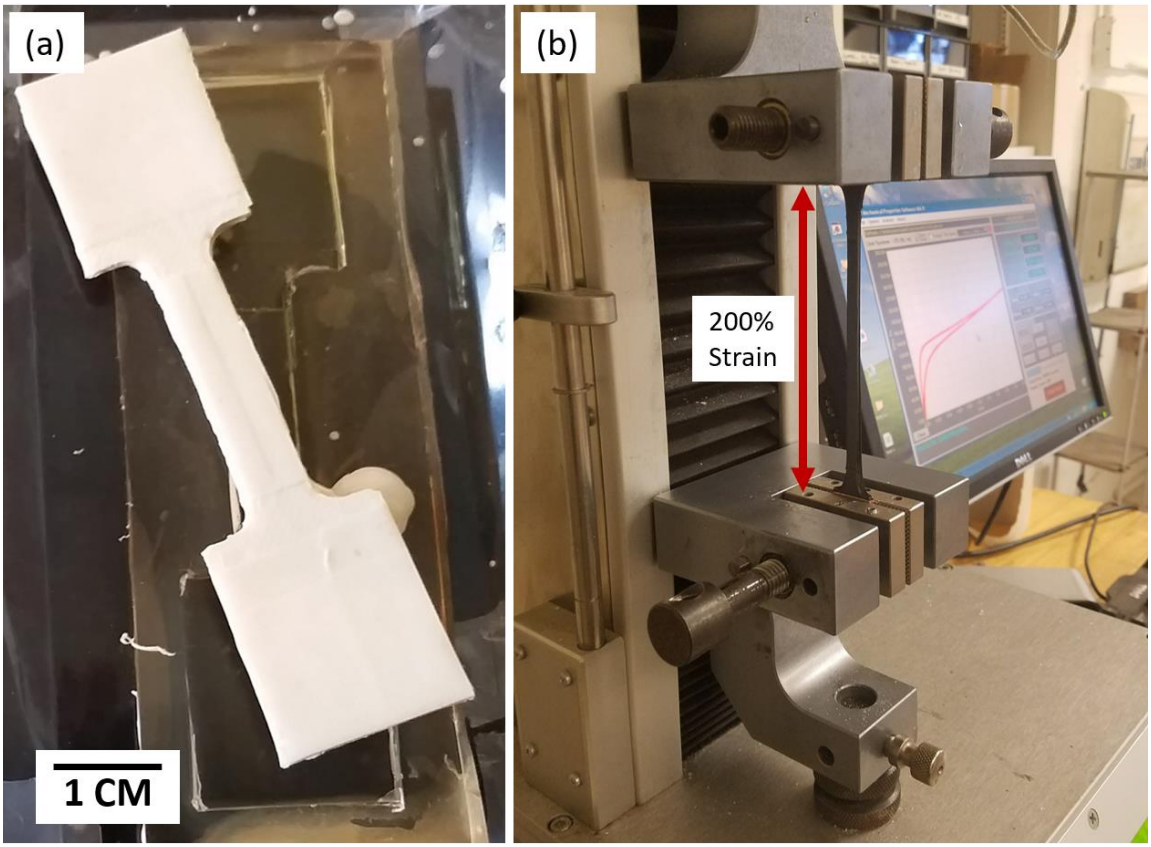

Figure 6: (a) Dog bone specimen of pure latex. (b) Dog bone specimen in tensile testing machine at strain of ~ 200%.

CHAPTER 3: RESULTS

3.1. Microstructure

3.1.1. Powders

Figure 7 shows SEM images and EDS analysis of Ni and InSb powders.

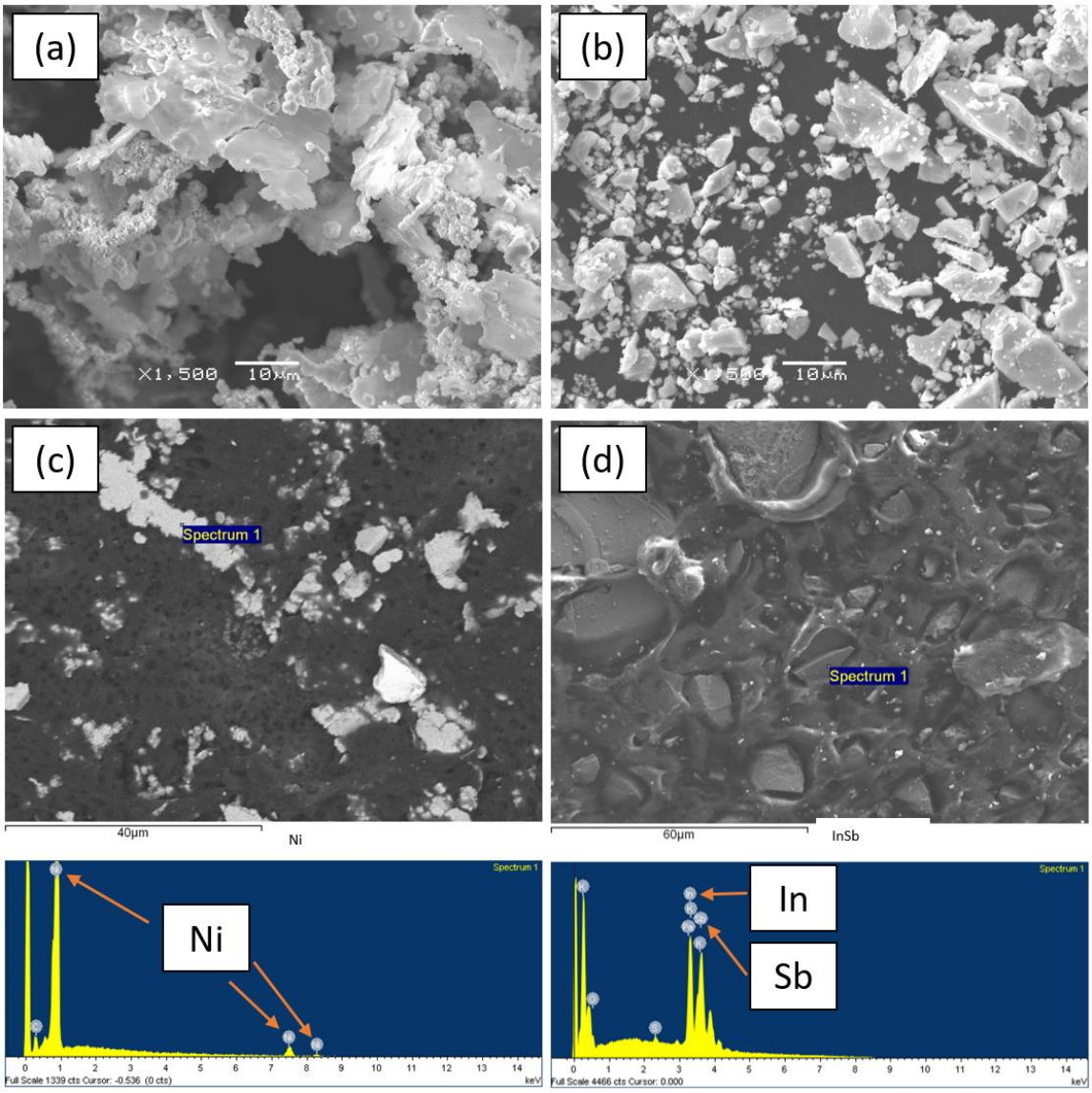

Figure 7: SEM images of (a) Ni powder and (b) InSb powder on adhesive carbon tape. EDS analysis on (c) Ni powder and (d) InSb powder on adhesive carbon tape. Credit: Ena Ibrisimovic.

Figure 7 shows that the Ni powder is very flake-like and larger than the InSb powder. Both powders have considerable particle size variance with some smaller than 1 μm and some larger than 20 μm. Figure 8 in Section 3.1.3. shows that the InSb particle size can approach 50 μm in some cases. The sharp edges and crystal facets of InSb powder suggest this material is crystalline with large grain size.

3.1.2. Ni-Latex Composites

Figure 8 and 9 present SEM images of Ni-latex composites at 17% and 25% powder concentrations, respectively. Due to the flake-like nature of the Ni powder, the particles laid flat on the surface of the composites, and are therefore not assumed to be an accurate representation of the vol.% of the sample. However, through these images, it is clear that higher concentrations of powder lead to more cracks and holes in the composite which could negatively impact the tensile strength.

The surfaces of both 17% and 25% Ni samples presented similar features in SEM analysis; see for comparison Figures 7(c) and 8(b). Small holes in the images are assumed to be due to the amount of water that had to be mixed in order to make the material pourable. On the 25 vol.% Ni sample, holes and cracks were discovered to be more prevalent and larger than the 17 vol.% Ni. This suggests a correlation between Ni concentration and the formation of defects, which also could explain why higher concentrations have lower fracture strength and elongation to fracture as shown in Section 3.4.

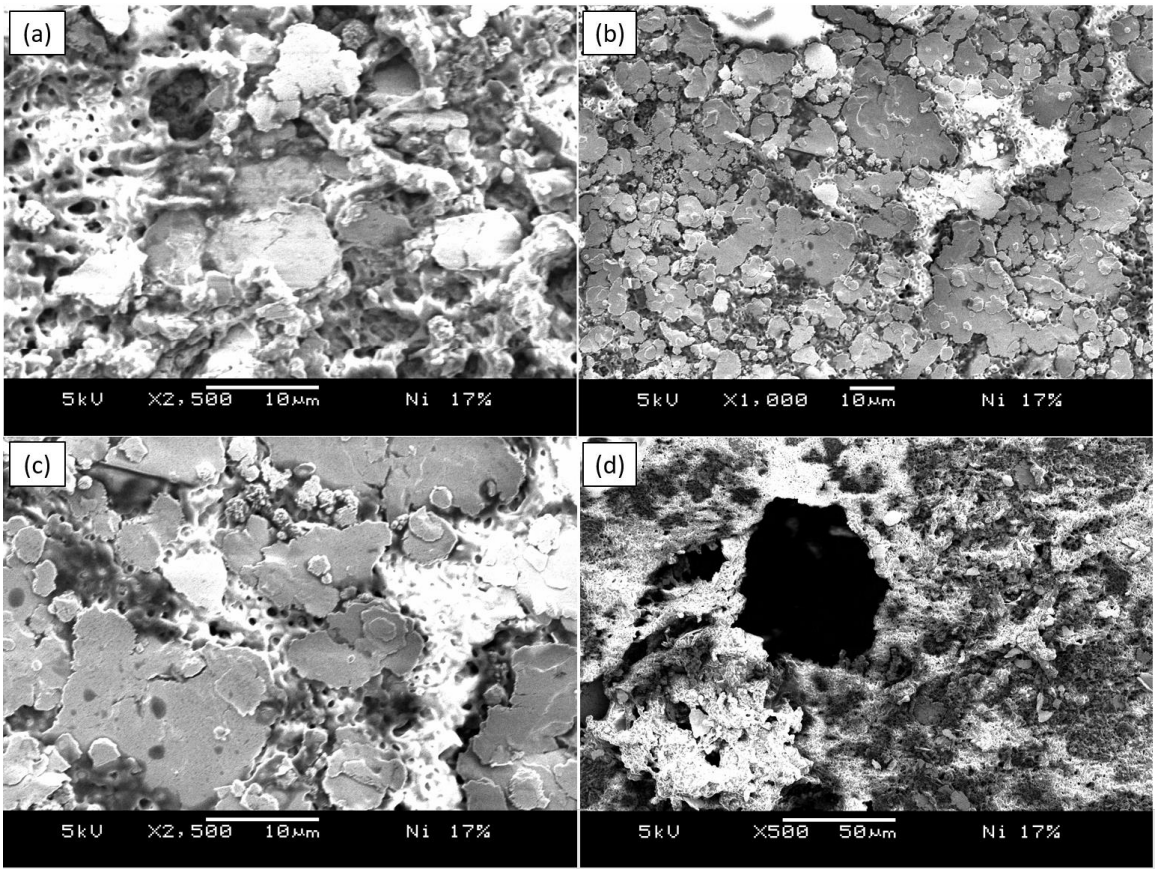

Figure 8: Surface SEM images of Ni-Latex composite at 17 vol.% Ni. Image (d) shows a hole formed when drying

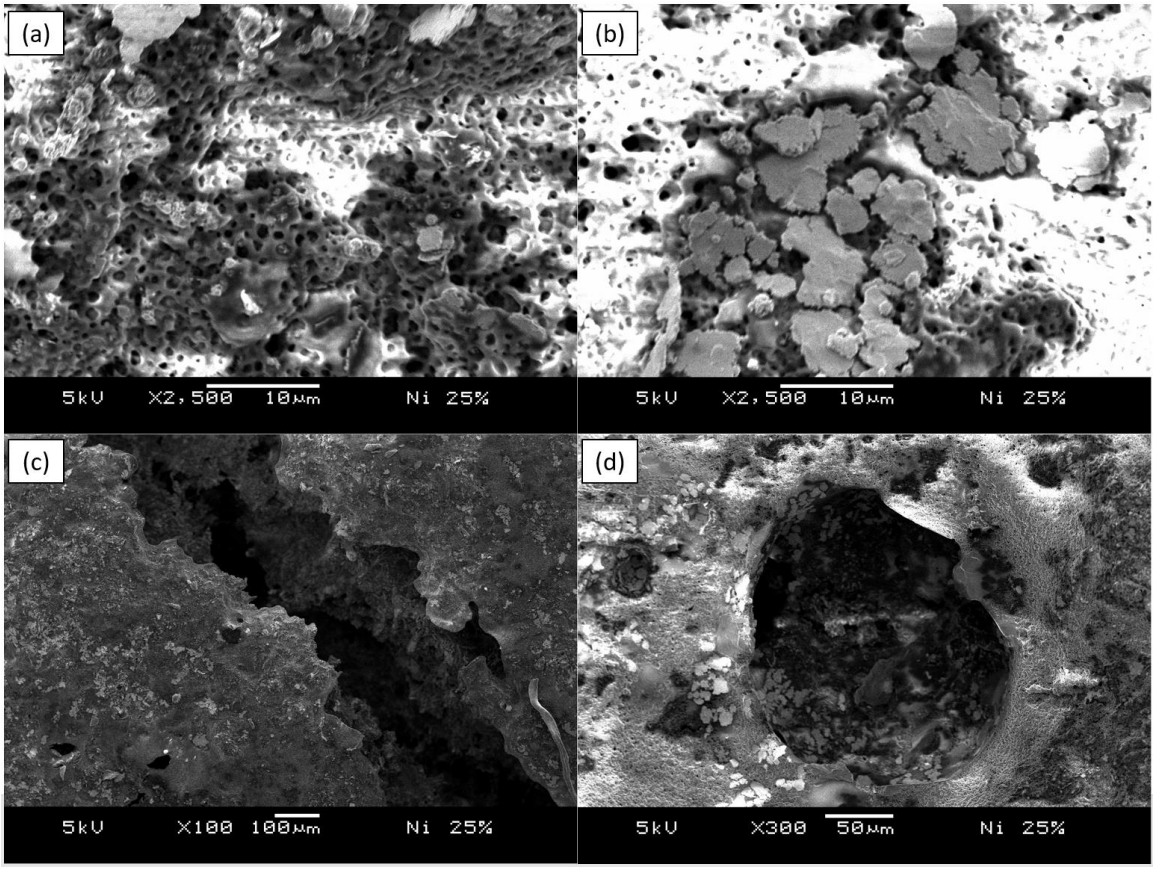

Figure 9: Surface SEM images of Ni-Latex composite with 25 vol.% Ni. Images (c) and (d) show very large crack and hole at high Ni concentration.

3.1.3. InSb-Latex Composites

Figures 10, 11 and 12 show SEM images of InSb-Latex composites at 17, 25, and 36 vol.% powder, respectively. The InSb particles are smaller than Ni ones, which seemed to cause less defects at higher concentrations. The cross section in Figure 9 shows that the particles are evenly distributed throughout the specimen and no settling occurs. Also, the large defects found in the same concentration of Ni (25 vol.%) were not observed. InSb-latex composites at the highest concentration tested as seen in Figure 10 (36 vol.%), did not display the cracks and holes that the 25 vol.% Ni sample showed.

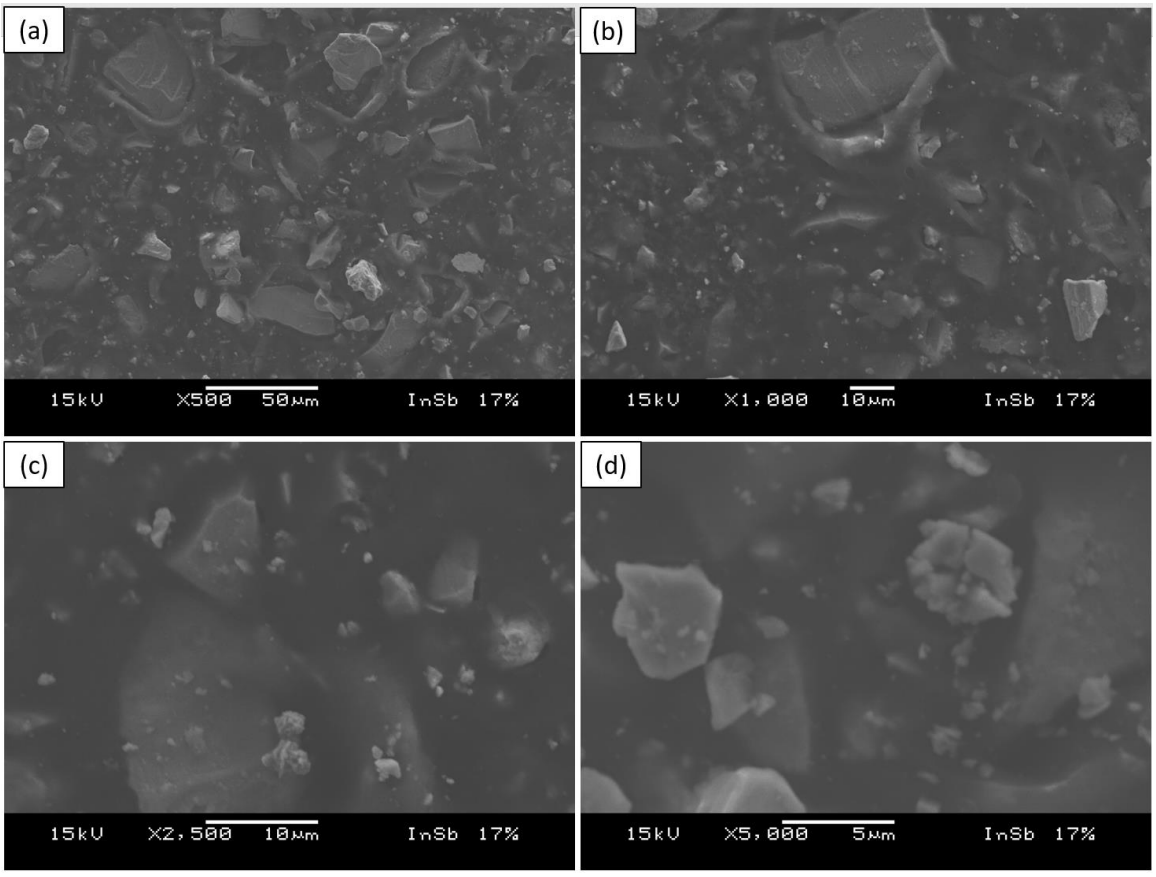

Figure 10: SEM images of InSb-Latex composites at 17 vol.% InSb.

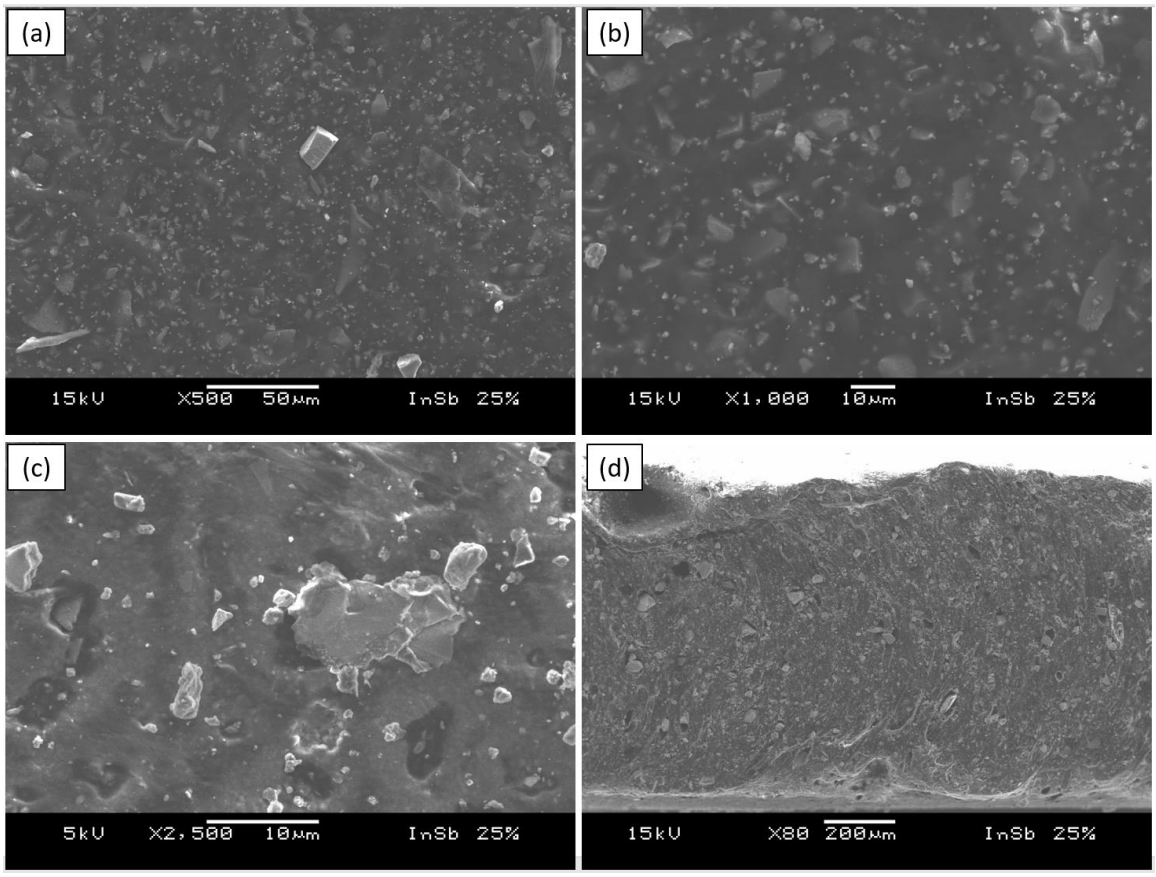

Figure 11: SEM images of InSb-Latex composites at 25 vol.% InSb. (d) Cross section view of the sample.

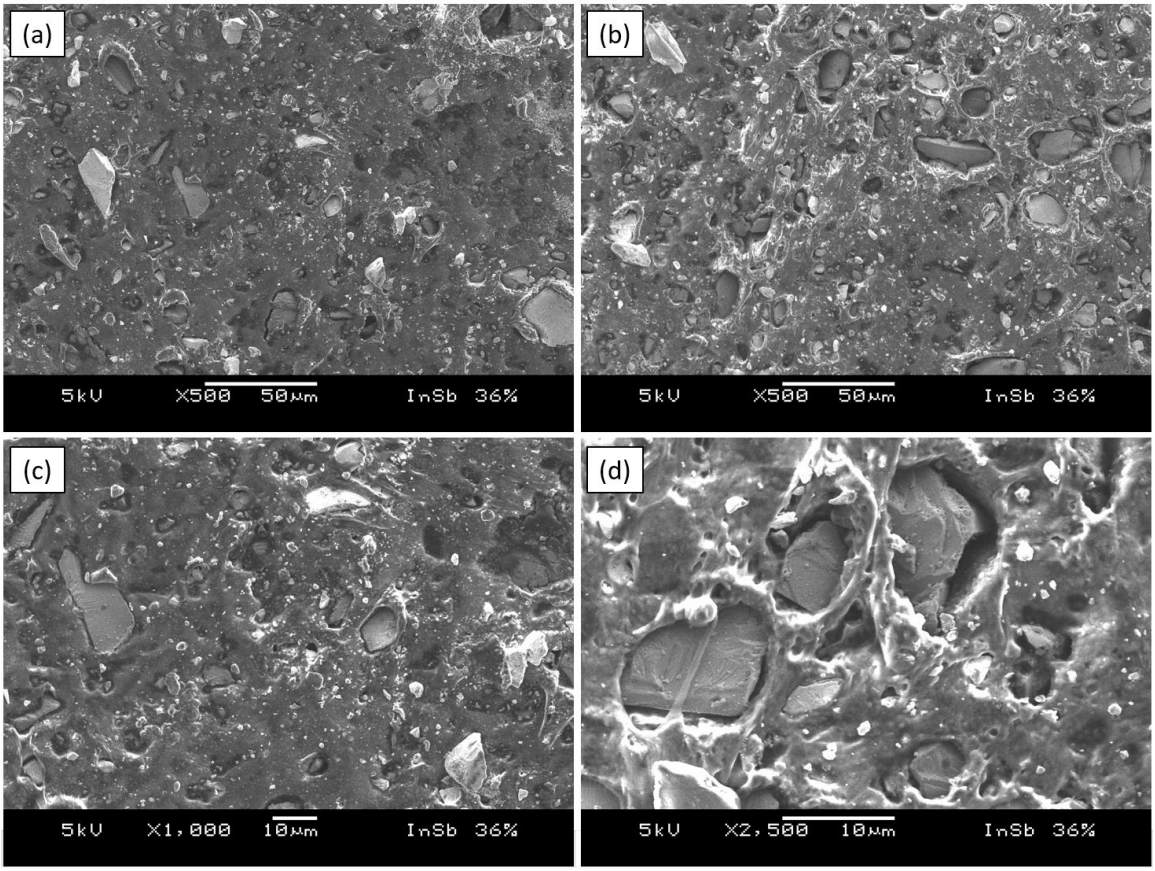

Figure 12: SEM images of InSb-Latex composite with 36 vol.% InSb.

3.1.4. Image Analysis

Figure 13 shows two SEM images with the Gwyddion mask applied and their corresponding particle size distributions. With Gwyddion image analysis, four SEM images of 17 vol.% InSb composite were analyzed and the average area covered by the mask was 19.4% with a standard deviation of 1.8%. This value is close to the theoretical vol.% calculated. Higher concentrations were also analyzed, but larger differences were found quantitatively with the theoretical values. This suggests that this method is not necessarily a good way to determine vol.%, because it is two-dimensional.

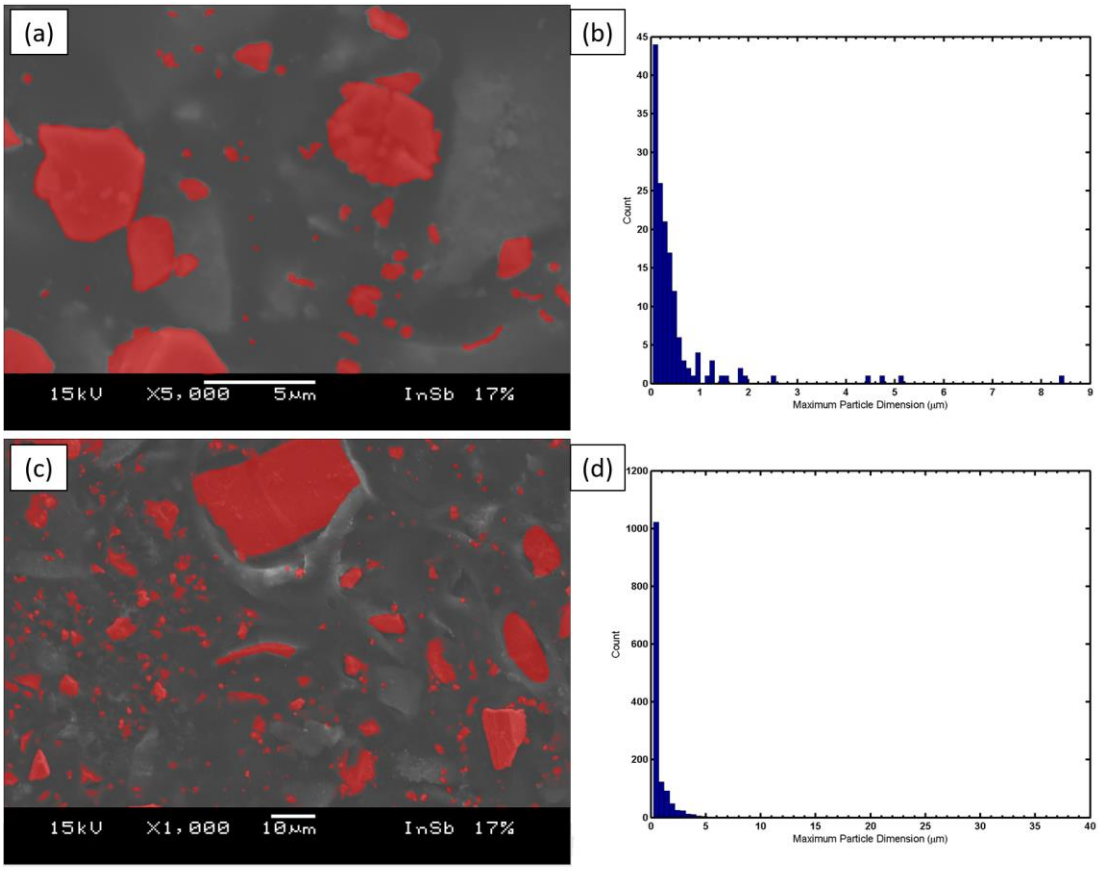

Figure 13: (a) SEM image of 17 vol.% InSb-latex composite with added Gwyddion mask. This particular mask was found to cover 17.8% of the area. (b) Histogram of the particle sizes in (a). (c) SEM image of 17 vol.% InSb-latex composite with added Gwyddion mask. This mask was found to cover 17.6% of the area. (d) Histogram of the particle sizes in (b).

3.2. Electrical Conductivity

Figure 14 shows the electrical conductivity of the composites for different vol.% powder. The Ni-latex composites showed higher conductivities at lower powder concentrations than those measured in InSb-latex composites, which is attributed to large differences in bulk electrical conductivity, 1.56 x 10^7 S/m and 2 x 10^4 S/m for Ni and InSb, respectively [26, 31]. A strong dependence of electrical conductivity on powder concentration is evident with the significant increase of conductivity over short increases of vol.%, however there appears to be a limit as the Ni-latex starts to plateau above 15 vol.%. This could be due to the appearance of cracks in the surface of the composite as shown in Figure 9.

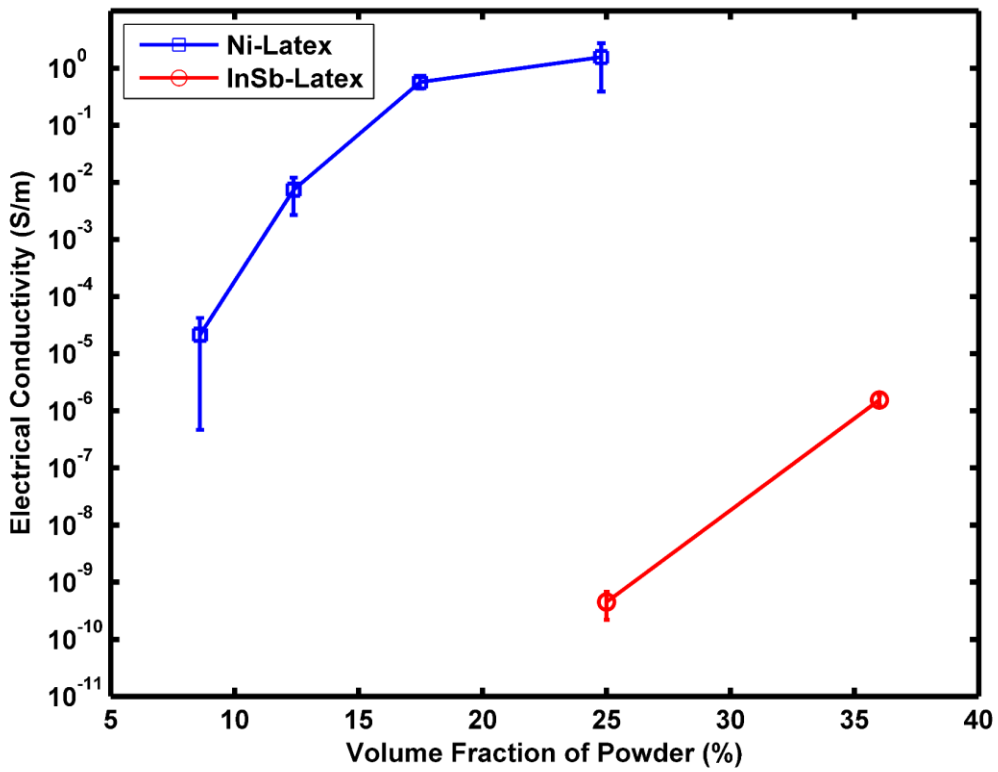

Figure 14: Electrical conductivity (S/m) of Ni and InSb latex composites at room temperature. Error bars represent one standard deviation.

3.3. Thermal Conductivity

Figure 15 shows the bulk thermal conductivity for different powder concentrations. Powder concentration seems to have little effect on the thermal properties of the composites. Though the bulk thermal conductivity values for Ni and InSb differ greatly, they have nearly identical values at the same concentration (17 vol.%). This suggests that thermal transport is mainly through the latex matrix and not the powder. The volumetric heat capacity (VHC) for InSb samples was found to be 1.25 MJ/m^{3}K and 1.43 MJ/m^{3}K for 25 vol.% and 36 vol.% InSb composites, respectively. For bulk InSb, bulk Ni, and pure latex, the VHC is ~832 kJ/m^{3}K, ~4.1 MJ/m^{3}K, and ~418.5 kJ/m^{3}K, respectively [26-28].

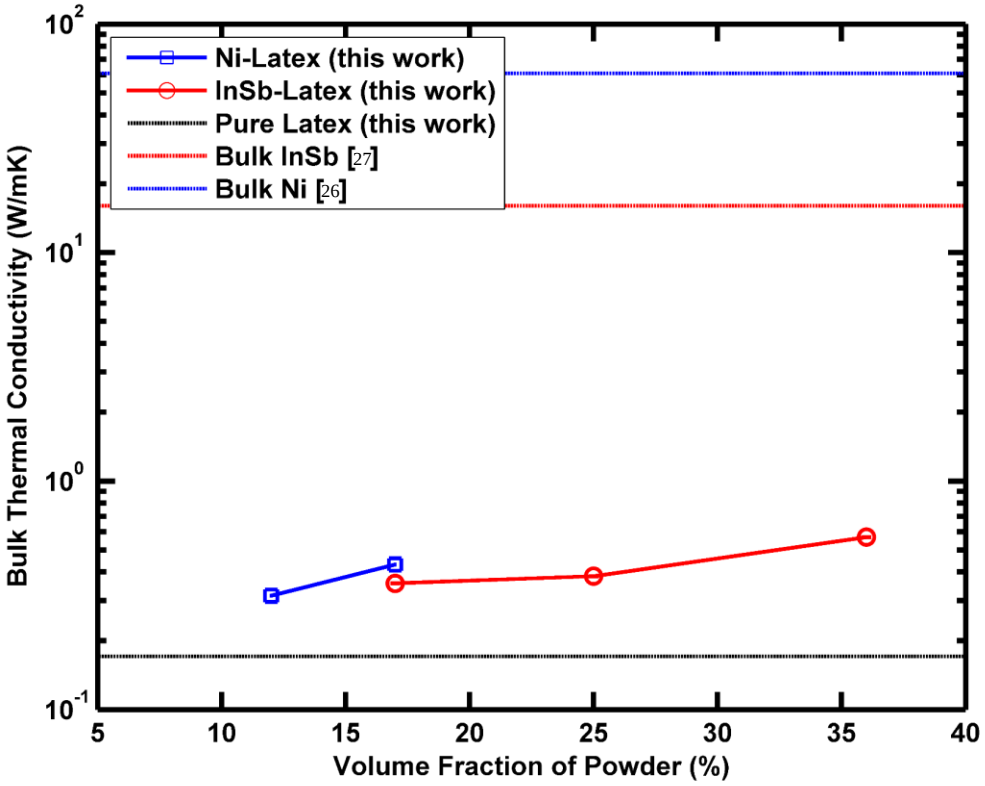

Figure 15: Bulk thermal conductivity of Ni and InSb latex composites at room temperature.

3.4. Mechanical Behavior in Tension

Figure 16 and 17 present the stress-strain curves for Ni-latex and InSb-latex composites at different vol.%, respectively. These figures show that the powder concentration has a large effect on fracture strength, but elastic behaviors show a similar trend for all samples. Figure 17 shows that the InSb composites have smaller fracture stress and elongation to failure as the volume fraction of powder increases.

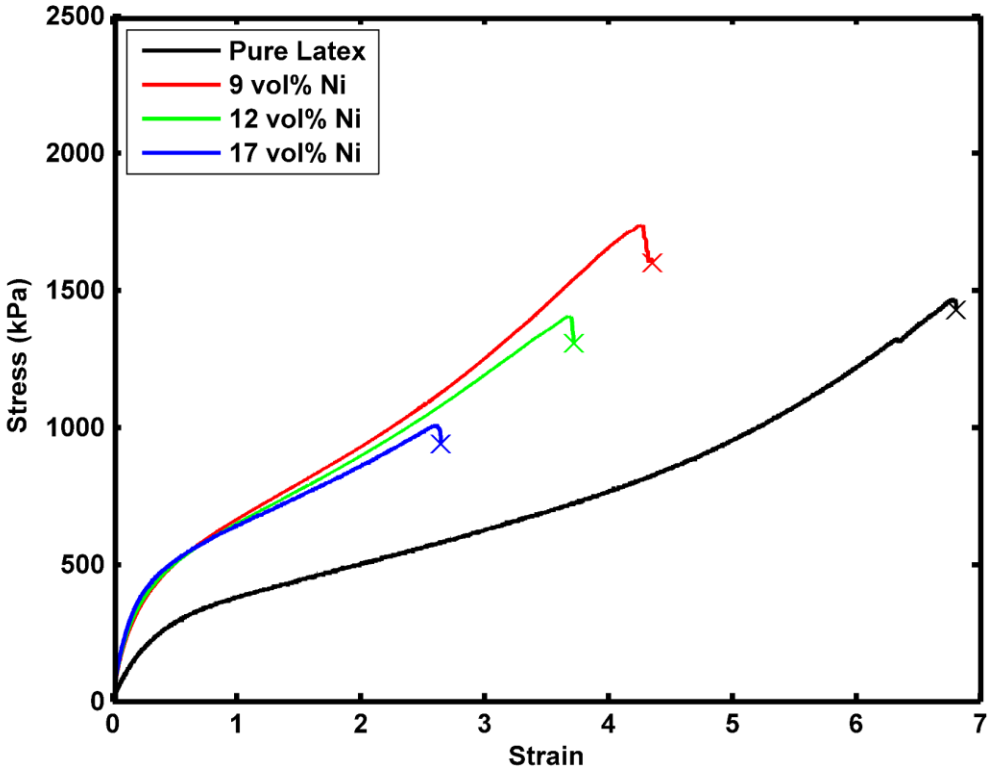

Figure 16: Stress-strain diagram for different concentrations of Ni powder and pure latex. Fracture is indicated by a cross symbol.

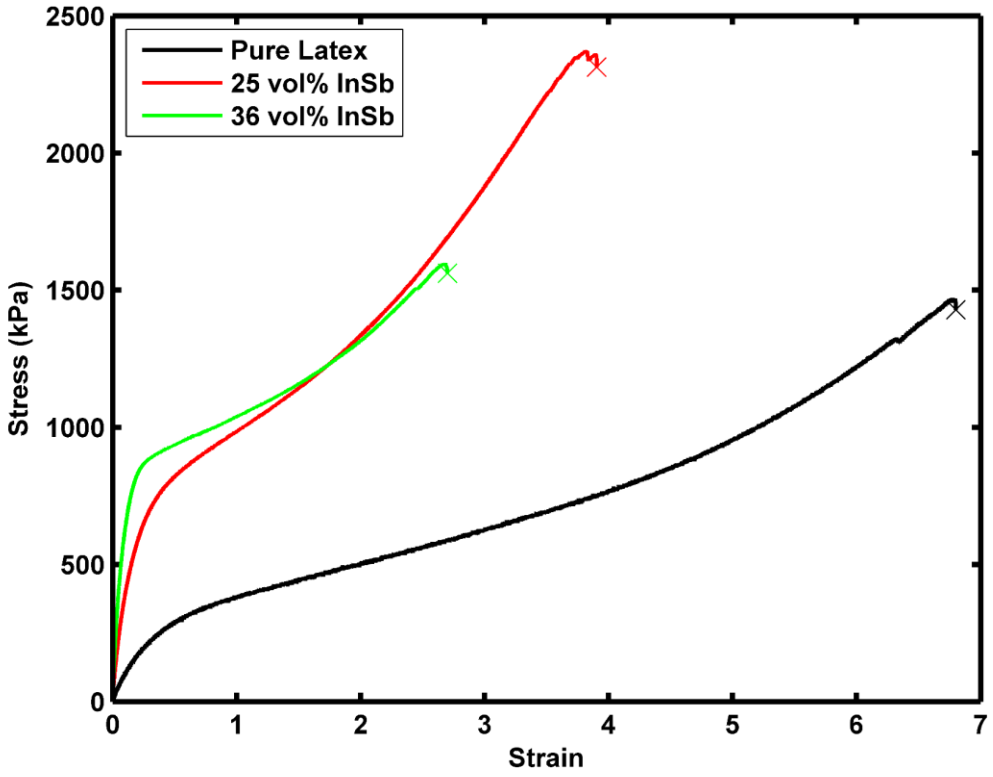

Figure 17: Stress-strain diagram for different concentrations of InSb powder and pure latex. Fracture is indicated by a cross symbol.

CHAPTER 4: DISCUSSION

4.1. Sample Continuity

Electrical conductivities of the thermal and mechanical specimens of the most conductive, stable sample (17 vol.% Ni) were measured to determine if the three samples demonstrated the same properties after drying in different molds. Three samples each were cut from the thermal and tensile specimens and measured with the same methods as the electrical samples. Figure 18 shows the average conductivities measured with error bars of 2 standard deviations. If the samples are normally distributed, then the conductivity measured will fall within 2 standard deviations approximately 95% of the time. Therefore, statistically, these three conductivities can be considered the same. This suggests that drying in different molds did not changed the overall structure of the composite.

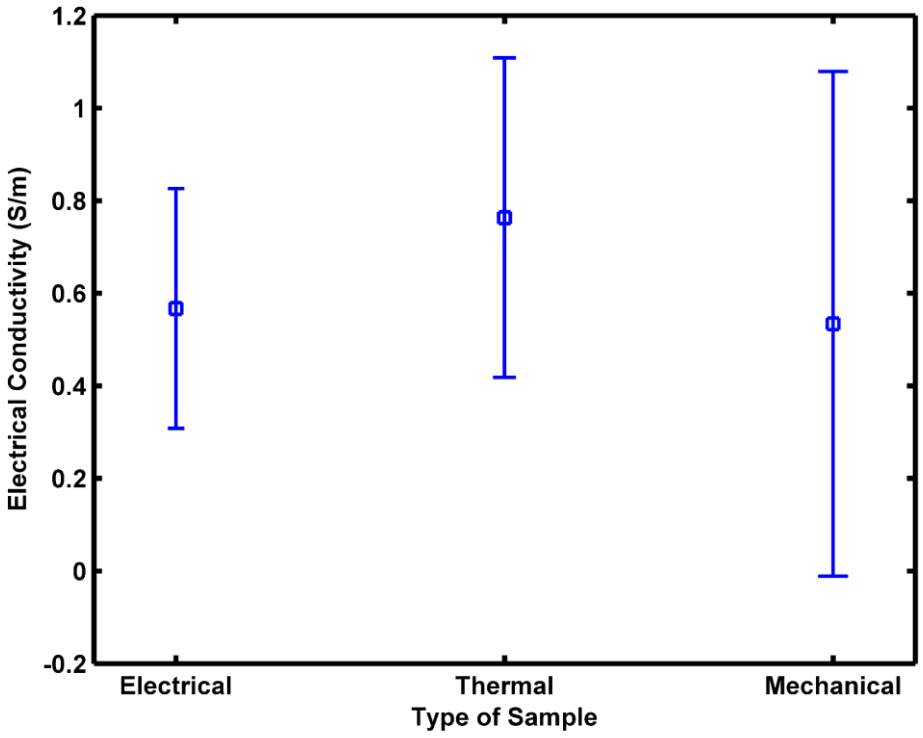

Figure 18: Comparison of electrical conductivities in 17 vol.% Ni electrical, thermal, and mechanical specimens. Error bars show 2 standard deviations.

4.2. Cracking Effects

At 25 vol.% Ni the latex matrix in the tensile specimens was unable to bind together well due to the large amount of Ni, cracked and fell apart as shown in Figure 19. For this reason, the thermal analysis was not done at this concentration, however, electrical data were obtained. It could be possible to make a tensile sample at 25 vol.% Ni concentration, but this would require changing the fabrication method from pouring the material into the mold some other method that doesn't require the material to be as thin, such as injection molding, which may change the morphology of the sample. InSb was found less conductive than Ni, but because the particle size was much smaller, higher concentrations up to 36 vol.% could be reached.

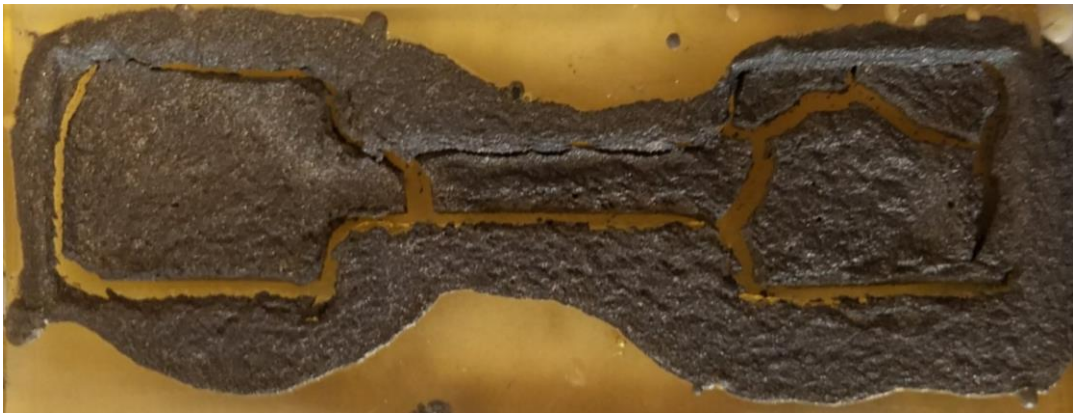

Figure 19: 25 vol.% Ni tensile specimen attempt cracked and fell apart in the mold while drying.

The Ni-latex composites showed significantly more formations of cracks and holes at higher powder concentrations than the InSb-latex composites. Even at the highest concentration studied, 36 vol.%, the InSb-latex surface was mostly smooth and free of cracks and holes. This is assumed to be a contributing factor in the tensile behavior of the samples. Water addition may play an important role in the formation of defects, however,

since water was added to both Ni and InSb samples, and fewer defects were observed in the InSb composites, particle shape and size is assumed to be the biggest factor.

4.3. Powder Concentration Effect

A large variance in particle size was found in both powders in Figures 6 and 12. It is unclear whether this has any effect on electrical conductivity. An attempt was made to grind the InSb powder with a mortar and pestle in hopes of decreasing particle size to improve the electrical conductivity but no differences were discovered, however there was not enough time or resources to investigate this further. Furthermore, the Ni particles were ~10x larger on average than the InSb particles and also much flatter and flake-like. This overall difference of particle size and shape between the two powders may explain the differences in microstructure and tensile performance. The Ni composites overall had lower fracture strength and tensile elongations at higher vol.% powder than the InSb composites. A Ni-latex tensile specimen was not even able to be made at the concentrations the InSb composites were created using the methods previously described.

Referring directly to Table 1, a few specimens were intentionally left out. With Ni-latex, at 9 vol.% the electrical conductivity was very low, unstable, and had high error. It was therefore decided not to measure the thermal conductivity at that concentration due to the uncertainty in the measurement. 17 vol.% InSb demonstrated no measurable electrical conductivity so a tensile specimen at that concentration was not created. A possible reason why these samples did not conduct well or at all could because there is just not enough powder in the composite to create pathways for electricity to flow. The percolation theory suggests that there is a critical concentration of particles in a matrix needed to create

interconnections all the way through a composite [32]. Additionally, the trend of the curve for electrical conductivity of Ni samples as a function of concentration closely resembles that of a CNT-polymer composite material demonstrated to have percolative character by Coleman et al including the fact that the electrical conductivity plateaus at higher concentrations. So this could explain why the electrical conductivity seems to plateau above 15 vol.% Ni.

The thermal conductivities of the different specimens did not differ greatly. The values resembled that of pure latex much more than either of the bulk conductivities. The 25 vol.% InSb specimen was purely isotropic thermally, however, 36 vol.% InSb started to show signs of anisotropy with an axial thermal conductivity of 0.453 W/mK and a radial thermal conductivity of 0.713 W/mK. This is still much closer to the bulk thermal conductivity of latex than that of bulk InSb, which suggests that the majority of heat transport is through the latex matrix instead of the conductive particles. This is promising for a TE material as low thermal conductivity is desired.

4.4. Ratio vs. Elongation

Table 2 shows a property summary for bulk and composite materials. Elongation to fracture for bulk InSb was estimated by dividing yield stress by Young's Modulus found in the literature [33, 34]. Figure 20 presents the ratio of electrical conductivity to thermal conductivity as a function of elongation to fracture. The ratio of electrical conductivity to thermal conductivity in Ni-latex composites saw a 2-order of magnitude increase from 12 vol.% to 17 vol.%. That same ratio saw an increase of 3 orders of magnitude in InSb-latex composites from 25 vol.% to 36 vol.%. Such large gains are realized by the fact that the

electrical conductivity has a very large dependence on powder concentration, but thermal conductivity does not. This allowed for a significant increase in electrical conductivity without noticeably raising the thermal conductivity which could vastly increase ZT values of these composites. Bulk InSb has the highest ratio, but very low elongation to failure. From 25 vol.% to 36 vol.%, the ratio increases by ~10^4, but elongation to failure only decreases by ~1.2. This shows great promise for a stretchable and flexible TE material because it maintains most of the stretchability of the latex and as powder concentration increases, approaches the ratio of bulk InSb.

Table 2: Property summary for bulk and composite materials

Material	σ (S/m)	k (W/mK)	ε_f (%)	σ/k
Bulk InSb	$2x10^4$ [31]	16 [27]	0.0145 [33,34]	$1.25x10^3$
Bulk Ni	$1.67x10^7$ [26]	60.7 [26]	30 [26]	$2.75x10^5$
Bulk Latex	$1x10^{-13}$ [28]	0.1707	680	$5.86x10^{-13}$
12 vol.% Ni	$7.37x10^{-3}$	0.3145	372	$2.34x10^{-2}$
17 vol.% Ni	$5.67x10^{-1}$	0.4309	265	1.32
25 vol.% InSb	$4.49x10^{-10}$	0.383	391	$1.17x10^{-9}$
36 vol.% InSb	$1.55x10^{-6}$	0.568	270	$2.73x10^{-6}$

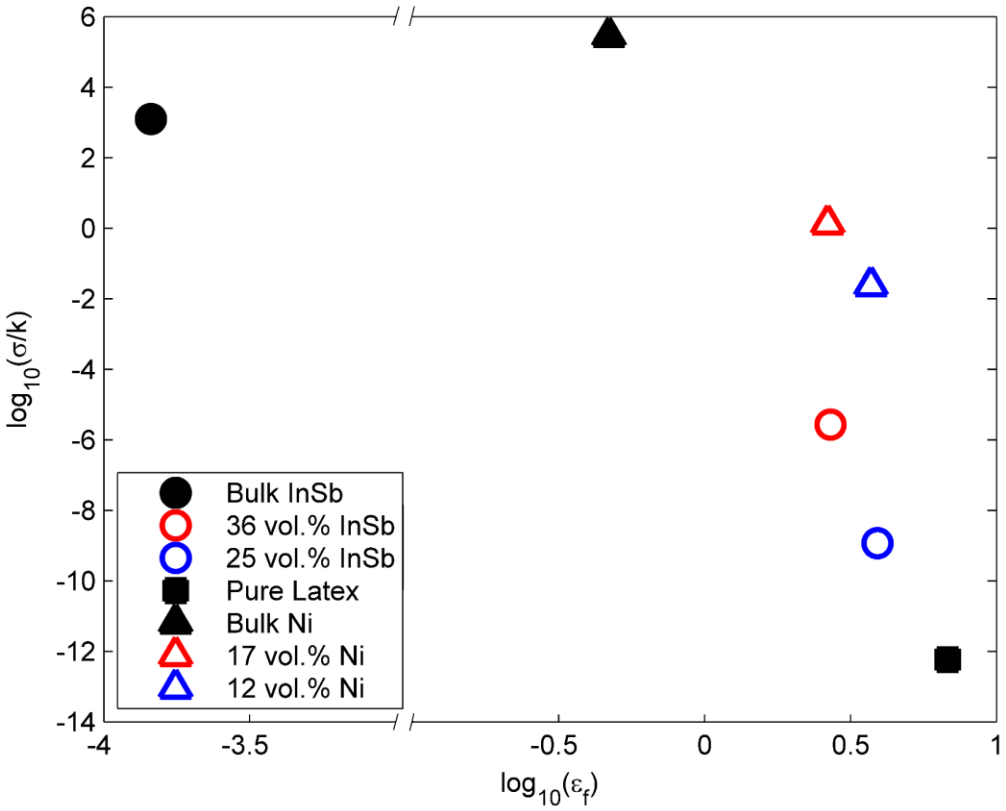

Figure 20: Ratio of electrical conductivity to thermal conductivity (σ/k) as a function of elongation to failure (εf) for bulk InSb, bulk Ni, and their latex-based composites.

CHAPTER 5: CONCLUSION

Stretchable latex-based conductive composites consisting of two powders, Ni and InSb, were synthesized. The effects of powder concentration on the electrical conductivity, thermal conductivity and tensile mechanical behavior were studied for different volume fractions of powder up to 36 vol.%.

Strong dependences of mechanical and electrical properties on powder concentration were found. By contrast, thermal conductivity was observed to remain low at all concentrations, suggesting that the predominant heat transport process is through the low-conductivity latex matrix rather than the conductive particles. This is especially good for thermoelectric applications as high electrical conductivity and low thermal conductivity are desired. Having large gains in electrical conductivity with minimal gains in thermal conductivity, and also maintaining a large amount of elongation to fracture show great promise for InSb-latex composites as stretchable thermoelectric materials.

Further investigation into these types of composites should focus on studying the Seebeck coefficient to calculate a figure of merit. This will be an excellent way to determine if this new material could potentially be used in stretchable thermoelectric devices for wearable electronics.

REFERENCES

[1] F. Xu and Y. Zhu, "Highly Conductive and Stretchable Silver Nanowire Conductors," *Advanced Materials,* vol. 24, pp. 5117-5122, 2012.

[2] J. Liang, K. Tong and Q. Pei, "A Water-Based Silver-Nanowire Screen-Print Ink for the Fabrication of Stretchable Conductors and Wearable Thin-Film Transistors," *Advanced Materials,* no. 28, pp. 5986-5996, 2016.

[3] M. Amjadi, A. Pichitpajongkit, S. Lee, S. Ryu and I. Park, "Highly Stretchable and Sensitive Strain Sensor Based on Silver Nanowire--Elastomer Nanocomposite," *American Chemical Society NANO,* vol. 8, no. 5, pp. 5154-5163, 2014.

[4] H. Wu, Y. Huang, F. Xu, Y. Duan and Z. Yin, "Energy Harvesters for Wearable and Stretchable Electronics: From Flexibility to Stretchability," *Advanced Materials,* no. 28, pp. 9881-9919, 2016.

[5] T. Starner, "Human-powered wearable computing," *IBM Systems Journal,* vol. 35, no. 3&4, pp. 1-12, 1996.

[6] Y.-H. Choi, M.-g. Kim, D.-H. Kang, J. Sim, J. Kim and Y.-J. Kim, "An electrodynamic preconcentrator integrated thermoelectric biosensor chip for continuous monitoring of biochemical process," *Journal of Micromechanics and Microengineering,* vol. 22, no. 045042, pp. 1-13, 2012.

[7] J. p. Rojas, D. Conchouso, A. Arevalo, D. Singh, I. G. Foulds and M. M. Hussain, "Paper-based origami flexible and foldable thermoelectric nanogenerator," *Nano Energy,* vol. 31, pp. 296-301, 2017.

[8] P. Lee, J. Lee, H. Lee, J. Yeo, S. Hong, K. H. Nam, D. Lee, S. S. Lee and S. H. Ko, "Highly Stretchable and Highly Conductive Metal Electrode by Very Long Metal Nanowire Percolation Theory," *Advanced Materials,* no. 24, pp. 3326-3332, 2014.

[9] M. S. White, M. Kaltenbrunner, E. D. Glowacki, K. Gutnichenko, G. Kettlgruber, I. Graz, S. Aazou, C. Ulbricht, D. A. M. Egbe, M. C. Miron, Z. Major, M. C. Scharber, T. Sekitani, T. Someya, S. Bauer and N. S. Sariciftci, "Ultrathin, highly flexible and stretchable PLEDs," *Nature Photonics,* vol. 7, pp. 811-816, 2013.

[10] Y. Sun, W. M. Choi, H. Jiang, Y. Y. Huang and J. A. Rogers, "Controlled buckling of semiconductor nanoribbons for stretchable electronics," *Nature Nanotechnology,* vol. 1, pp. 201-207, 2006.

[11] D.-Y. Khang, J. A. Rogers and H. H. Lee, "Mechanical Buckling: Mechanics, Metrology, and Stretchable Electronics," *Advanced Functional Materials,* vol. 19, pp. 1526-1536, 2009.

[12] D.-H. Kim, Y.-S. Kim, J. Wu, Z. Liu, J. Song, H.-S. Kim, Y. Y. Huang, K.-C. Hwang and J. A. Rogers, "Ultrathin Silicon Circuits With Strain-Isolation Layers and Mesh Layouts for High-Performance Electronics on Fabric, Vinyl, Leather, and Paper," *Advanced Materials,* no. 21, pp. 3703-3707, 2009.

[13] S. P. Lacour, J. Jones, S. Wagner, T. Li and Z. Suo, "Stretchable Interconnects for Elastic Electronic Surfaces," *Proceedings of the IEEE,* vol. 93, no. 8, pp. 1459-1467, 2005.

[14] H. Cheng, J. Wu, M. Li, D.-H. Kim, Y.-S. Kim, Y. Huang, Z. Kang and K. C. Hwang, "An analytical model of strain isolation for stretchable and flexible electronics," *Applied Physics Letters,* vol. 98, no. 061902, 2011.

[15] L. Liang, C. Gao, G. Chen and C.-Y. Guo, "Large-area, stretchable, super flexible and mechanically stable thermoelectric films of polymer/carbon nanotube composites," *Journal of Materials Chemistry C,* no. 4, pp. 526-532, 2016.

[16] S. J. Kim, J. H. We and B. J. Cho, "A wearable thermoelectric generator fabricated on a glass fabric," *Energy & Environmental Science,* no. 7, pp. 1959-1965, 2014.

[17] B. Zhang, J. Sun, H. E. Katz, F. Fang and R. L. Opila, "Promising Thermoelectric Properties of Commercial PEDOT:PSS Materials and Their Bi2Te3 Powder Composites," *Applied Materials & Interfaces,* vol. 2, no. 11, pp. 3170-3178, 2010.

[18] W. Liu, X. Yan, G. Chen and Z. Ren, "Recent advances in thermoelectric nanocomposites," *Nano Energy,* vol. 1, pp. 42-56, 2012.

[19] M. Scheele, N. Oeschler, K. Meier, A. Kornowski, C. Klinke and H. Weller, "Synthesis and Thermoelectric Characterization of Bi2Te3 Nanoparticles," *Advanced Functional Materials,* vol. 19, no. 21, p. 3476–3483, 2009.

[20] S. K. Mishra, S. Satpathy and O. Jepsen, "Electronic structure and thermoelectric properties of bismuth telluride and bismuth selenide," *Journal of Physics: Condensed Matter,* vol. 9, no. 2, p. 461–470, 1996.

[21] X. B. Zhao, X. H. Ji, Y. H. Zhang, T. J. Zhu, J. P. Tu and X. B. Zhang, "Bismuth telluride nanotubes and the effects on the thermoelectric properties of nanotube-containing nanocomposites," *Applied Physics Letters,* vol. 86, no. 062111, 2005.

[22] S. Yamaguchi, T. Matsumoto, J. Yamazaki, N. Kaiwa and A. Yamamoto, "Thermoelectric properties and figure of merit of a Te-doped InSb bulk single crystal," *Applied Physics Letters*, vol. 87, no. 20, p. 201902, 2005.

[23] R. Bowers, R. W. Ure Jr., J. E. Bauerle and A. J. Cornish, "InAs and InSb as Thermoelectric Materials," *Journal of Applied Physics*, vol. 30, no. 6, pp. 930-934, 1959.

[24] "Voyager: The Interstellar Mission," NASA: Jet Propulsion Laboratory, 2017. [Online]. Available: http://voyager.jpl.nasa.gov/.

[25] V. Leonov and R. J. M. Vullers, "Wearable electronics self-powered by using human body heat: The state of the art and the perspective," *Journal of Renewable and Sustainable Energy*, vol. 1, p. 062701, 2009.

[26] "Material Data Sheet - Nickel," MatWeb Material Property Data, 2017. [Online]. Available: http://www.matweb.com/search/DataSheet.aspx?MatGUID=e6eb83327e534850a062dbca3bc758dc.

[27] "Material Data Sheet - Indium Antimonide," MatWeb Material Property Data, 2017. [Online]. Available: http://www.matweb.com/search/DataSheet.aspx?MatGUID=b37307e599924e93ba57765351e3b794.

[28] "Material Data Sheet - Natural Rubber," MatWeb Material Property Data, 2017. [Online]. Available: http://www.matweb.com/search/DataSheet.aspx?MatGUID=da912e0c50154649a201d8f7abbf7e90.

[29] D. Necas and P. Klapetek, "Gwyddion: an open-source software for SPM data analysis," *Central European Journal of Physics*, vol. 10, no. 1, pp. 181-188, 2012.

[30] V. Bohac, M. K. Gustavsson, L. Kubicar and S. E. Gustafsson, "Parameter estimations for measurements of thermal transport properties with the hot disk thermal constants analyzer," *Review of Scientific Instruments*, vol. 71, no. 6, pp. 2452-2455, 2000.

[31] W. D. Callister and D. G. Rethwisch, Fundamentals of Materials Science and Engineering - An Integrated Approach, Wiley, 2015.

[32] J. N. Coleman, S. Curran, A. B. Dalton, A. P. Davey, B. McCarthy, W. Blau and R. C. Barklie, "Percolation-dominated conductivity in a conjugated-polymer-carbon-nanotube composite," *Physical Review B*, vol. 58, no. 12, 1998.

[33] D. Varshney, G. Joshi, M. Varshney and S. Shriya, "Pressure induced structural phase transition and elastic properties in BSb, AlSb, GaSb and InSb compounds," *Physica B: Condensed Matter,* vol. 405, no. 7, pp. 1663-1676, 2010.

[34] I. Yonenaga, "Mechanical Properties and Dislocation Dynamics in III-V Compounds," *Journal de Physique III,* vol. 7, pp. 1435-1450, 1997.

[35] V. Leonov, "Thermoelectric Energy Harvesting of Human Body Heat for Wearable Sensors," *IEEE Sensors Journal,* vol. 13, no. 6, pp. 2284-2291, 2013.

[36] Y. Du, S. Z. Shen, K. Cai and P. S. Casey, "Research progress on polymer-inorganic thermoelectric nanocomposite materials," *Progress in Polymer Science,* vol. 37, pp. 820-841, 2012.

[37] Y. P. Mamunya, V. V. Davydenko, P. Pissis and E. V. Lebedev, "Electrical and thermal conductivity of polymers filled with metal powders," *European Polymer Journal,* vol. 38, pp. 1887-1897, 2002.

[38] R. W. Keyes, "Effect of Pressure on the Electrical Conductivity of InSb," *Physical Review,* vol. 99, no. 2, pp. 490-495, 1955.

[39] D. Merkel, *Fabrication and Testing of Flexible Indium Antimonide Nanowire Networks,* University of Vermont, 2014.

[40] H. J. Hrostowski, F. J. Morin, T. H. Geballe and G. H. Wheatley, "Hall Effect and Conductivity of InSb," *Physical Review,* vol. 100, no. 6, pp. 1672-1676, 1955.

[41] W. Thongruang, R. J. Spontak and C. M. Balik, "Bridged double percolation in conductive polymer composites: An electrical conductivity, morphology, and mechanical property study," *Polymer,* vol. 43, pp. 3717-3725, 2002.

[42] M. Gustavsson, E. Karawacki and S. E. Gustafsson, "Thermal conductivity, thermal diffusivity, and specific heat of thin samples from transient measurements with hot disk sensors," *Review of Scientific Instruments,* vol. 65, no. 12, pp. 3856-3859, 1994.

[43] W. J. Xie, J. He, S. Zhu, X. L. Su, S. Y. Wang, T. Holgate, J. W. Graff, V. Ponnambalam, S. J. Poon, X. F. Tang, Q. J. Zhang and T. M. Tritt, "Simultaneously optimizing the independent thermoelectric properties in (Ti,Zr,Hf)(Co,Ni)Sb alloy by in situ forming InSb nanoinclusions," *Acta Materialia,* vol. 58, no. 14, p. 4705–4713, 2010.